Postirradiation characterization of palladium as an additive for fuel cladding chemical interaction mitigation in metallic fuel

Fidelma G. Di Lemma[a], Tammy M. Trowbridge[a], Luca Capriotti[a*], Jason M. Harp[b], Michael T. Benson[a], and. Robert D. Mariani[a]

[a] Idaho National Laboratory, Idaho Falls, ID 83415, USA
[b] Oak Ridge National Laboratory, Oak Ridge, TN 37831, USA

*Corresponding Author Contact Information:
Dr. Luca Capriotti
Characterization and Advanced PIE Division,
Material Fuel Complex,
Idaho National Laboratory
P. O. Box 1625 MS 6000,
Idaho Falls, ID 83415-6000 U.S.A.
Phone: +1 (208) 533-7080
E-mail: luca.capriotti@inl.gov

For submission to *Journal of Nuclear Materials*
July 2021

KEYWORDS
Metallic fuel, advanced fuel design, PIE, FCCI, additives, Pd.

ABSTRACT
This work describes the microstructural and elemental characterization of irradiated metallic fuels containing palladium as an additive. The use of additives has been proposed to control Fuel-Cladding Chemical Interaction (FCCI) and thus to promote higher fuel utilization (i.e., higher burnup). In this work, Pd has been investigated as a potential additive to metallic fuel to bind lanthanides, impeding their migration and attack on the cladding. The influence of Pd on the microstructure, chemistry and performance of metallic fuel has been characterized via scanning electron microscopy for two metallic fuel designs—namely, annular and solid fuel. Pd was observed to play an important role in the chemistry of the fuel. Indeed, the addition of Pd leads to the formation of new phases. Pd was detected to combine not only with the lanthanides, as intended, but also with Zr, a main element of the fuel matrix. While Pd proved to be effective in preventing lanthanide migration and their attack on the cladding, the Pd-Zr compound may potentially lead to other unexpected fuel-performance issues, such as the formation of low-melting point phases and increased unalloyed U available for FCCI interaction with Fe in the cladding. Even the increase of Zr to 13wt%. did not completely mitigate this adverse phenomenon generated by the Pd-Zr interaction. Thus, the efficacy of using this additive needs further investigation.

1. INTRODUCTION

One feasible option for future commercialization of advanced reactor design is the Sodium-cooled Fast-Reactor (SFR) concept. Metallic–fuel-based SFRs have various positive characteristics [1–4] that encourage this concept's deployment. They possess favorable neutronic feedback [2] that makes them "inherently safe." Their application for actinide transmutation promotes a closed nuclear fuel cycle; thus, it improves waste minimization with particular application to long-lived actinides, such as Pu and Am [3,4]. Moreover, their breeding capabilities could lead to minimize any future limitation of nuclear fuel supply [4]. Metallic fuel also possesses good material properties for application in nuclear reactors, such as high thermal conductivity and high fissile density. One of the major limitations encountered with the use of metallic fuel in SFRs is related to its chemical compatibility with the cladding. This phenomenon is currently limiting metallic-fuel burnup extension, which is already high at 10% FIMA for the Department of Energy (DOE)-qualified U-10Zr alloy design [5]. Indeed, at burnups over 5% FIMA, Fuel Cladding Chemical Interaction (FCCI) has been observed under normal operation in metallic fuel (U-Zr and U-Pu-Zr) systems [6]. FCCI has been associated with the interaction of U and Pu with Fe present in the martensitic stainless-steel cladding (HT9). Lanthanides (Ln) such as Ce, La, Nd and Sm were also observed to aggravate FCCI, promoting an increase in the thickness of the interaction layer [7]. These Ln are the predominant elements generating FCCI in U-Zr fuels during normal operation, as they lanthanides migrate fast in the fuel and diffuse rapidly into cladding [8]. FCCI affects strongly fuel performance as the interaction layer formed may be brittle; thus, it can weaken the cladding mechanical properties. Cracks in the cladding have been observed in the FCCI region and may lead to cladding failure. Moreover, low-melting temperatures phases have been observed to form due to these chemical interactions (e.g., U_6Fe, Pu_6Fe, $LnFe_2$ and Ln_2Fe_{17}) [6, 8] contributing to cladding wastage. This eutectic phase may melt and lead to thinning of the cladding and its rupture, For these reasons, the FCCI region in the cladding has been considered as "wastage" because it does not serve a safety function and does not contribute to overall cladding strength [6,9]. FCCI is thus a safety concern at burnups higher than 10% FIMA, especially in view of unexpected transient conditions related to accidents [6], which can lead to loss of the cladding containment characteristic.

Various approaches have been considered to prevent or minimize FCCI. These include a physical barrier between the fuel and cladding (e.g., Zr-rich "rind" and cladding liners) or elements added during fuel fabrication to bind lanthanides and to minimize their migration (a.k.a. immobilize) towards the cladding [8–9]. In this second approach, Pd has been proposed as a dopant because of thermodynamic analyses of its potential behavior and observed low-migration behavior in irradiated fuel [9]. It was thought that Pd presented a compromise of the desired properties for additivities, such as low fast-neutron capture cross-section, high affinity with lanthanides to form stable compounds, a corresponding weaker chemical reactivity with fuel constituents, low additive-to-lanthanide stoichiometry, and uniform distribution in the fuel [8]. Indeed Ln-Pd compounds have been observed to form in irradiated fuel. However, the amount of Pd produced during fission is inadequate to bind and immobilize lanthanides; thus, for Pd to be an effective additive, additional Pd must be alloyed in the fuel.

While various studies have investigated Pd as an additive in unirradiated fuel [8–13], minimal data has been published on irradiated metallic fuel with such additives [13–16]. This paper examines and reports, for the first time, the influence of Pd as an additive in different concentrations on the microstructure and composition of irradiated metallic fuel via Scanning Electron Microscopy (SEM). The samples analyzed in this study were obtained from the Advanced Fuel Campaign (AFC) series 3 experiments (AFC-3A, AFC-3B, AFC-3D), irradiated at Idaho National Laboratory's (INL's) Advanced Test Reactor (ATR) [15,17]. These

experimental campaigns aimed to increase the fuel-performance envelope of metallic fuel alloys for SFR by exploring different fuel concepts and fuel designs, such as solid vs annular fuel. Annular fuel has been proposed for improved geometrical stability at low smear densities [16]. Smeared density is defined (%) as the cross-sectional area ratio of the fuel slug to the cladding inside**.** Moreover, annular fuel design as the potential to eliminate sodium bonding while still maintaining good heat-transfer properties [16]. Annular metallic fuels can also eliminate the fuel-cladding gap, mitigating slumping concerns. Such annular design may allow a fuel to achieve ultrahigh burnup (30-40%) without limitations from Fuel-Cladding Mechanical Interaction (FCMI), which was one of the limiting phenomena in the first application of metallic fuel due to fuel swelling leading to excessive cladding strain and breaching the fuel pin [1]. Moreover, by the addition of Pd to annular fuel it may be possible to limit also FCCI. This work evaluates the effectiveness of Pd addition as an FCCI mitigator in both fuel designs through Post-Irradiation Examination (PIE).

2. Experimental work

2.1 Fuel alloys fabrication

The fabrication process of the fuel rods and details on the specimens analyzed in this work are described in Ref. [18]. All alloys were fabricated via arc melting. Homogenization was achieved through repeated melts. The alloys were then cast into quartz molds using a counter-gravity injection casting system where a vacuum was used to draw the alloy melt into the mold [15]. The annular fuel geometry was obtained using molds containing an inner quartz core, with subsequent removal by drilling. The outside of the annular slugs was machined to the desired outer diameter for AFC-3D. This final machining was on the other hand not performed for the AFC-3B series fuel fabrication and may have influenced final dimension tolerance in the fuel rods. The fuel slugs were then cut to length, inserted into the cladding material (HT-9) with an inner diameter of 4.95 mm and an outer diameter of 5.84 mm. Next they were either bonded with sodium (solid fuel) or helium (annular). When sodium was used, the rodlet was filled before welding the top end cap. The sodium settled by heating the welded rodlet in a well furnace followed by gentle tapping. Further information on rodlets characteristics are reported by Harp et al. [15], and details on pre-irradiation characterization and engineering scale PIE can be found in Refs. [15,17,19]. A summary of the rodlets analyzed in this study and their characteristics are described in Table 1.

Table 1. List of rodlets analyzed in this study and their characteristics.

Sample Name	AFC ID	Composition (%wt.)	Fuel Form	Bond Element	Nominal smeared density (%)	Outer Diameter (mm)	Inner Diameter (mm)
ANN-4Pd-10Zr	*AFC-3B-R2*	U-4Pd-10Zr	Annular	Helium	55	4.85	3.25
ANN-4Pd-13Zr	*AFC-3D-R5*	U-4Pd-13Zr	Annular	Helium	55	4.92	3.30
SOL-2Pd-10Zr	*AFC-3A-R5B*	U-2Pd-10Zr	Solid	Sodium	75	4.23	N/A
SOL-4Pd-13Zr	*AFC-3D-R2*	U-4Pd-13Zr	Solid	Sodium	55	3.66	N/A

2.2 Irradiation experiment, irradiation history and sample preparation

The described fuel alloys were irradiated at INL's ATR. The fuel rods were irradiated in a double

encapsulated set-up with a stainless steel 316 capsule and a Cd shroud. The Cd shroud creates the desired radial power profile that is prototypic of fast-reactor conditions. The SS316 capsule provides temperature control across the gap between the rodlet and the external capsule. Moreover, it is the primary safety barrier between the experiment and the ATR coolant. Details on irradiation and on the capsule design can be found in the work of Harp et al. [15,17]. The validity of this encapsulation method as representative of fast irradiation conditions has been evaluated in Ref. [20].

The irradiation parameters applied to the selected rods are shown in Table 2. Temperature in the fuel rods, in terms of time averaged and maximum Peak Inner-Cladding Temperature (PICT), are listed in Table 2. Details on heat generation and Linear Heat Generation Rate (LHGR) are described by Harp et al. [15, 17] and reported in Table 2. Temperature calculations performed with a finite element analysis code (Abaqus [21]) with the generation of correlations between LHGR and PICT as described by Harp et al. [17]. Samples were chosen for these analyses as they presented similar burnups and temperatures. This study meant to investigate the effect of different fuel design (namely solid fuel vs. annular fuel) and different additive concentrations on fuel microstructure and performance

Table 2. Irradiation conditions as obtained from Refs. [15,17]. PICT simulated values obtained from Abaqus have been averaged over the irradiation time.

Sample Name	AFC ID	Burnup (%FIMA)	PICT maximum (°C)	PICT averaged (°C)	LHGR averaged (W/cm)
ANN-4Pd-10Zr	*AFC-3B-R2*	3.6	575	535	330
ANN-4Pd-13Zr	*AFC-3D-R5*	2.9	610	580	345
SOL-2Pd-10Zr	*AFC-3A-R5B*	2.5	575	535	320
SOL-4Pd-13Zr	*AFC-3D-R2*	2.7	630	595	330

The samples analyzed in this study were obtained from the central axial position (x/L = 0.5, where x is the cut position and L is the full length of the fuel slug) of the described rodlets. The specimens were cut using a water-cooled slow-speed saw in a hot cell with a pure argon environment. They were then mounted in a stainless-steel mount with epoxy, ground, and finely polished to 1 μm. Final sample preparation was performed just before the microscopy analyses to minimize sample oxidation. The samples were downsized from the initial full cross-section to minimize radiation dose and permit further analyses via SEM, which will not have been possible with full size samples due to high radiation fields. Samples SOL-2Pd-10Zr and ANN-4Pd-10Zr were cut as strips, while ANN-4Pd-13Zr was cut in half (see Figure 1). Sample SOL-4Pd-13Zr was analyzed as a full cross section (as presented in Figure 1). Note that during downsizing, detachment of the cladding from the fuel appeared in sample ANN-4Pd-13Zr. This thus did not permit a clear analysis of the FCCI for this sample. Finally, the different mounts were coated with a thin gold layer to create a good electrical conductivity for SEM to be performed at INL's Electron Microscopy Laboratory (EML) of the Material Fuel Complex.

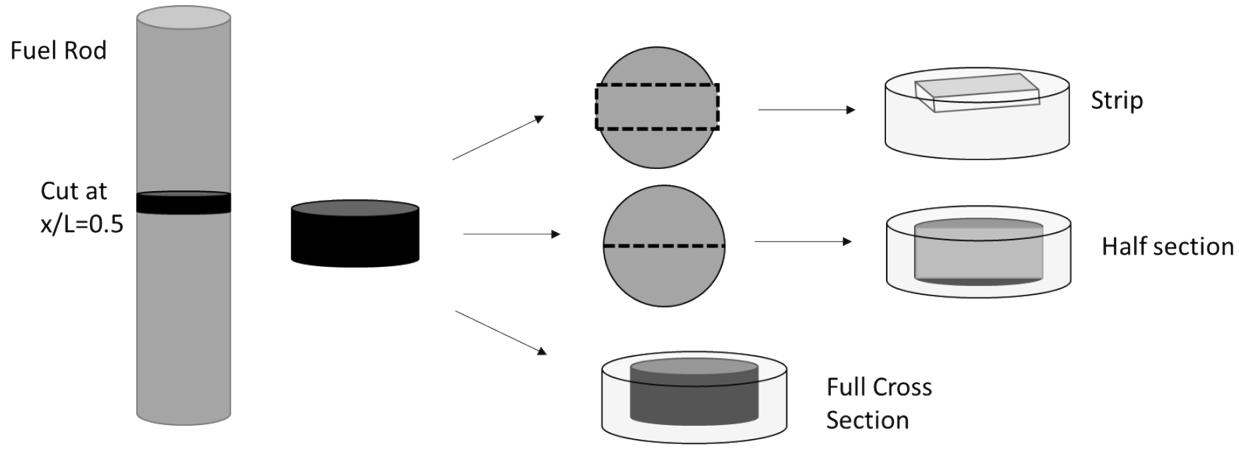

Figure 1-Cutting diagram for the samples and mounting technique.

2.3 Instrument and analyses

SEM was performed with a JEOL-7000 equipped with an Oxford Energy-Dispersive x-ray Spectrometer (EDS, X-max 50) for elemental analyses. Wavelength Dispersive x-ray Spectroscopy (WDS) with an Oxford Inca-Wave was used for peak overlap identification. Analyses were conducted at 20 keV. Current was optimized based on the analysis: for EDS, deadtime was maintained under 50% while, for WDS, the current was maximized for increased count rates. X-ray maps were collected with the EDS detector with a dwell time of 100 ms for a total of 10 frames and with a resolution of 512 × 384 pixels. Point analyses and line-scans were collected up to approximately 15 s live time for a total count of over 1 million for each spectrum. EDS analyses were conducted via standardless method. The described detectors (both EDS and WDS) are calibrated annually for reliable measurements. Images were collected in Secondary Electron (SE) mode for morphological information and in BackScattered Electron (BSE) mode for compositional information.

3. Results

3.1 Fuel microstructure and main element redistribution

The imaging of sample surfaces obtained by SEM indicates very different microstructures for the different specimens analyzed. Compositional differences can be observed by the variation of contrast in the BSE images forming different regions in the fuels' cross section.

3.1.1 Annular fuel

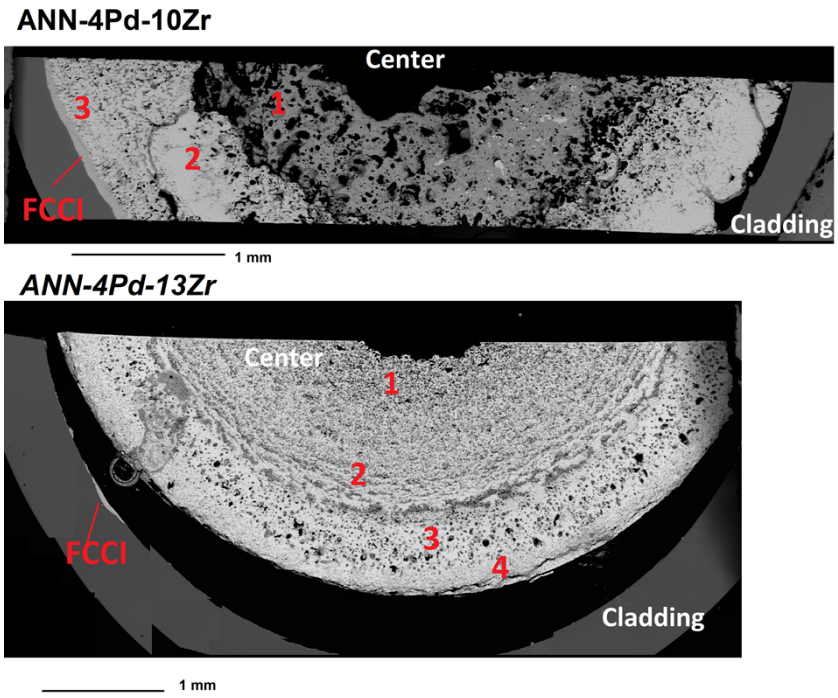

Figure 2. Overview of the microstructure in the annular samples collected in the BSE mode. The numbers in red indicate the different elemental-redistribution regions. Note that the fuel/cladding separation in sample ANN-4Pd-13Zr happened during sample preparation.

In both annular fuel specimens, it is noted that the anulus is not completely closed after irradiation (Figure 2), which is consistent with previous metallography analyses [15,17]. From the BSE imaging in Figure 2, it can be inferred that some element redistribution has occurred during irradiation. In Figure 2, it is observed that sample ANN-4Pd-10Zr shows qualitatively three areas of elemental redistribution. The first, more-internal region (1) is very dark, indicating the presence of elements with low mass number. The second and third regions (near the cladding) present similar contrast, but different microstructure with decreasing porosity. In the other annular specimen ANN-4Pd-13Zr four different regions were identified based on the microstructure (Figure 2). Here, the BSE contrast is less pronounced than in the other annular sample, possibly indicating a limited variation in composition. However, similar to the previous sample, the inner regions (1–2) present darker contrast with respect to the outer regions (3–4). In Region 1 of ANN-4Pd-13Zr, the porosity is spherical, which could be an indication of the formation of a gamma U region, consistent with previous metallic-fuel observations [1]. From Regions 1 to 4, various degrees of porosity are found along the radius. Region 2 presents elongated porosity of small dimension that could be related to a region with low Zr, while region 3 presents a highly elongated porosity configuration that may be indicative of the presence of orthorhombic alpha-U (α-U).

The analysis of the annular samples via EDS confirmed the elemental redistribution. Similar to previous experience with irradiated metallic fuels [1,15, 22–26], it was observed in these specimens that Zr and U redistribute in the fuel, with the central region being enriched in Zr. Such elemental diffusion phenomena, common in metallic fuels, are driven by temperature

gradients and enhanced by irradiation [27]. These chemical variations result in distinct radial zones of different compositions, which can affect the performance of the fuel. Indeed, fuel constituent migration affects its properties, including solidus and liquidus temperatures, thermal conductivity, along with mechanical properties, reaction rates, and radial power density profile [28]. Different phases are formed due to this elemental redistribution and are observed across the sample radius to vary both in composition and concentration. Zirconium enrichment in the central region, as observed in the annular samples, generally occurs when temperatures are higher than 650°C [1]. This is consistent with the temperature simulated by Abaqus for these experiments. The EDS analyses (Figure 3) detected in the most-internal region (Figure 2, region 1) the presence of two main phases for sample ANN-4Pd-13Zr. These were found to be: 1) a phase containing mainly U and 2) a dark-gray phase in higher fraction containing U-Zr (about 65U-35Zr wt%). In this region, precipitates were also observed. Of particular interest for this section is the presence of nearly pure Zr precipitates (over 90 wt%), which were observed to have generally a dendritic shape. This feature has been also reported in fresh fuel before irradiation and may be related to the fabrication process. It may be mentioned that precipitates previously reported for irradiated fuels [25–26] containing Zr-Ru were also observed throughout the samples but are not relevant in the current investigation of Pd effect.

Moving radially towards the cladding, similar phases to the one in region 1 can be observed. However, it was noticed that their abundancy changed (Figure 4, Region 2). In Region 2, the U phase seems to be in higher proportions than the U-Zr phase. This is consistent with the mentioned Zr redistribution behavior, which tends to be higher in the center and to decrease in the periphery of the fuel rod (toward the cladding). In the fuel a lamellar structure is developed between the U-Zr and the U phase, which may be related to eutectoid decomposition (α-U/δ-UZr_2) [29].

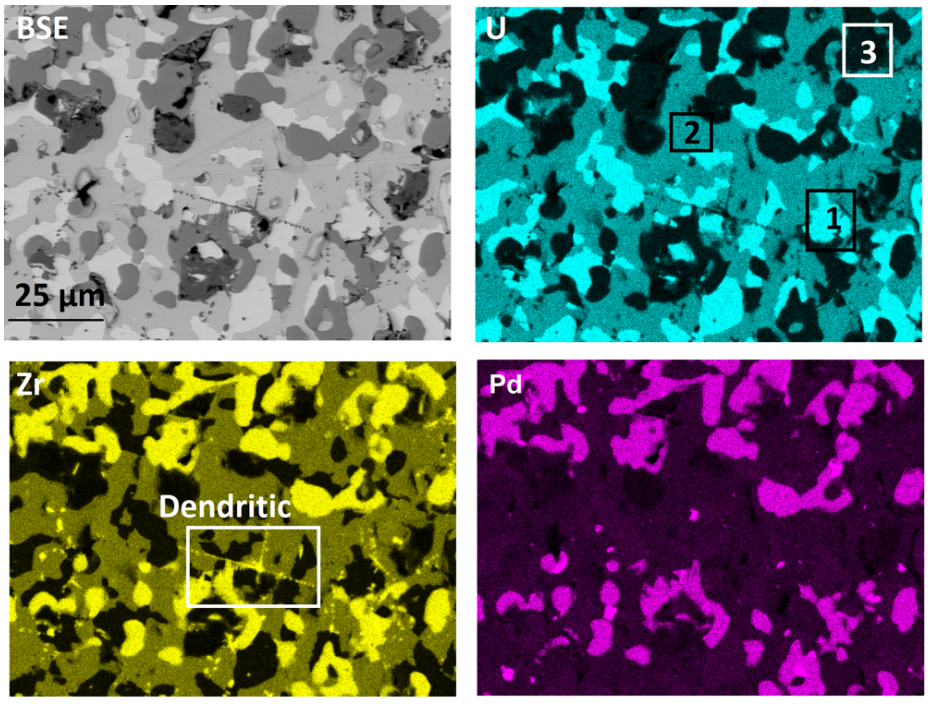

Figure 3. X-ray maps showing the different phases observed in the most-internal Region 1 for sample ANN-4Pd-13Zr. A U enriched phase (1), and a second phase higher in Zr content (2). A Pd-Zr phase is also observed. This last phase was also found in freshly cast fuel (3). Finally, the presence of Zr dendritic precipitates was observed.

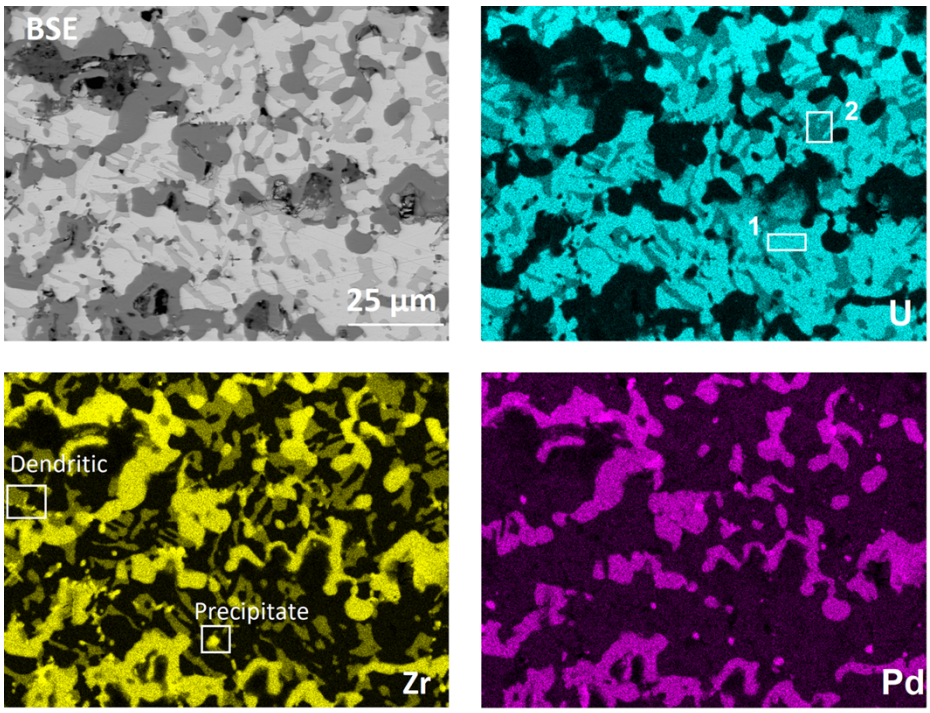

Figure 4-X-ray maps of the main elements present in sample ANN-4Pd-13Zr in Region 2 showing similar "phases" to Region 1. It can be observed that the fuel present two different phases, showing a kind of lamellar eutectoid structure with one region enriched in U (1) and the other enriched in Zr (2). Finally the Pd-Zr phase and Zr dentritic precipitates are again observed.

Sample ANN-4Pd-10Zr shows a very different elemental composition to the other samples, which was unexpected. High Fe content was observed in this sample, even in the central region. This affected the U-Zr phase in the central region (Region 1 in Figure 2). Detailed analysis (Figure 5) showed the U-Zr phase to be very complex and to contain up to 10 wt% Fe (50Zr-20U-20Pd-10Fe wt%). Moreover, the high amount of Fe in this specimen leads to the formation of abundant Zr-Fe precipitates in the other regions of the fuel. Indeed, Fe played an important role in this sample, forming phases that were not observed in the other specimens. Although this phenomenon was unforeseen, one possible explanation of the high Fe content in the fuel may be related to the fabrication process. For early annular fuel rodlets (as in AFC Series B), fabrication of the fuel slugs involved casting them into annular molds. The quartz molds were broken off the slugs, and the slugs were placed in the pins with a significant gap (>50 µm) between the fuel slug and the cladding [15]. In the AFC-3D experiment, the fuel slugs were machined after casting, as mentioned previously, to create a small (<25 µm) controlled gap between the fuel and the cladding. The larger (not predicted at the time) fuel/cladding gap could have deteriorated the fuel performance in reactor with temperature regimes higher compared to the calculated temperatures listed in Table 2. Imperfect fuel cladding contact can increase fuel temperature. In Beausoleil et al. [30] it is discussed in detail how asymmetric behavior in the fuel/cladding gap closure, as the one proposed for ANN-4Pd-10Zr, can lead to increased temperatures where the fuel and cladding are in contact when double encapsulation method is applied as in these experiments. This higher-than-expected temperature at the fuel/cladding gap may have driven higher amounts of Fe to migrate into the fuel reaching the central region.

In this sample (ANN-4Pd-10Zr), the U-enriched phase (U>95 wt%. Figure 5) seems to be present in low concentration in the central region (Region 1 in Figure 2) and in the form of

precipitates, rather than a homogeneous main phase as observed in sample ANN-4Pd-13Zr. This nearly pure U phase is then absent in the second region, where the main phase always contains U and Zr alloyed together.

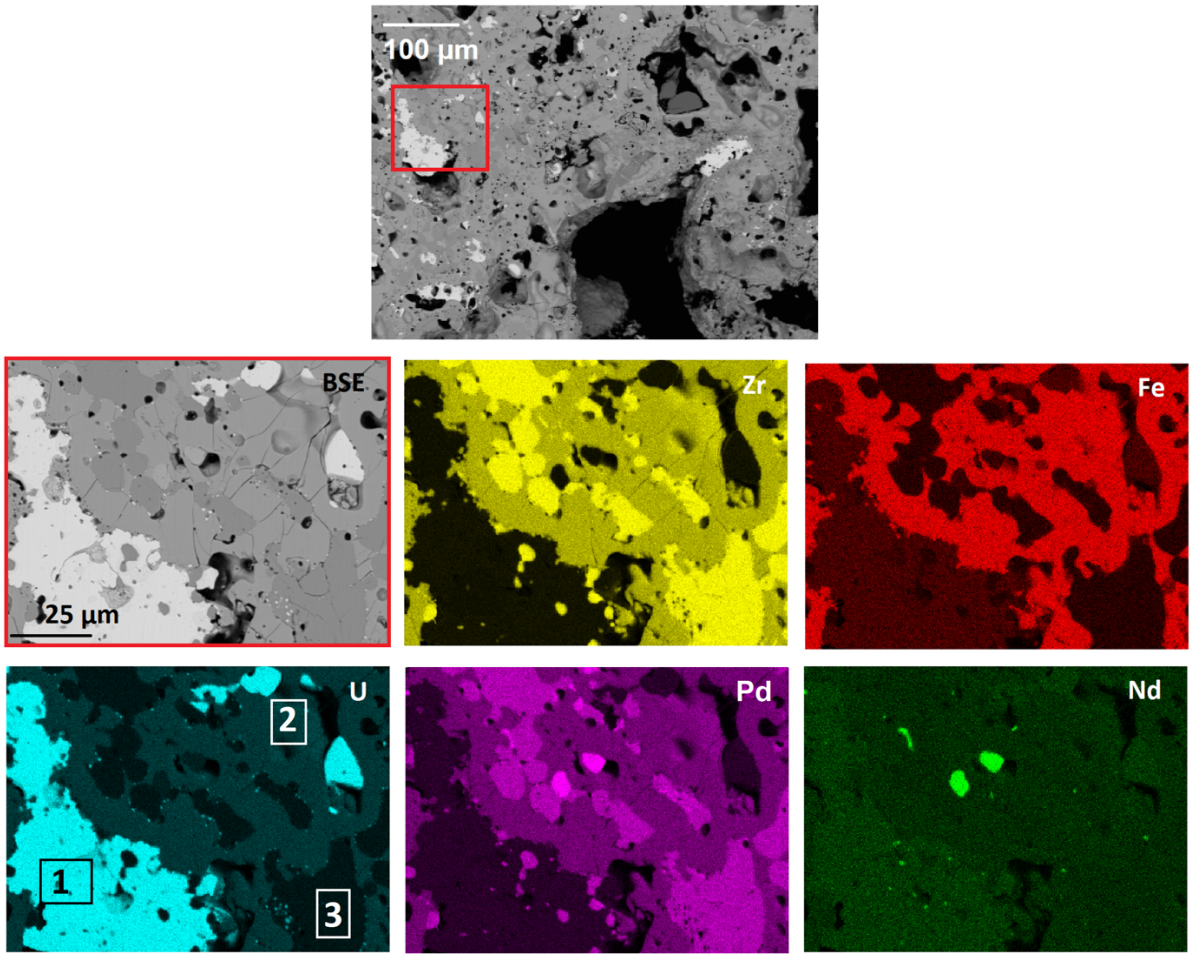

Figure 5. BSE images at different magnifications and X-ray maps, showing a different chemistry for sample ANN-4Pd-10Zr in the internal region (Region 1). The U phase (1) is a minor phase, while the predominant U-Zr phase (2) contains a high amount of Fe. A Pd-Zr phase is also observed in high concentration (3). Some lanthanides are observed in this region to be immobilized together with Pd in precipitates; an example is shown for Nd.

Finally, for both annular fuels (ANN-4Pd-13Zr-Figure 6 and ANN-4Pd-10Zr-Figure 7), the outer regions are shown to be composed of a main phase of nearly pure U with a secondary phase containing U-Zr (with Zr around 10 wt%). For sample ANN-4Pd-10Zr, this second U-Zr phase is present in lower amounts, which is in line with the lower Zr composition of sample ANN-4Pd-10Zr's with respect to ANN-4Pd-13Zr (10 wt% in ANN-4Pd-10Zr vs. 13 wt% in ANN-4Pd-13Zr).

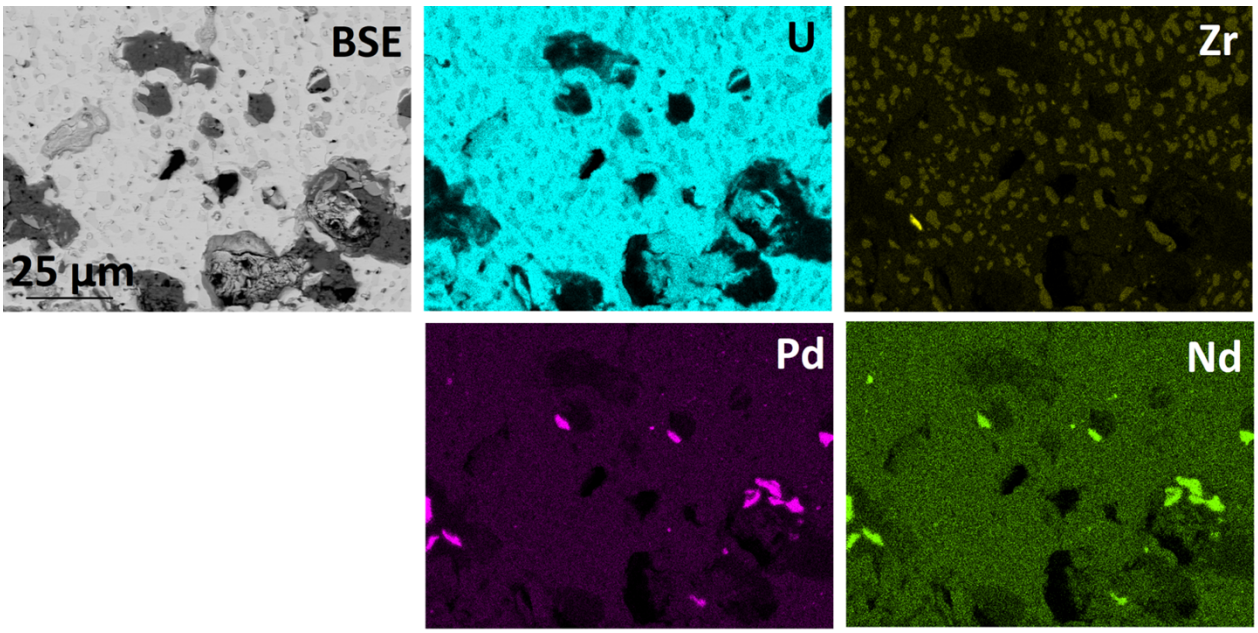

Figure 6. X-ray maps showing the two-phase region in sample ANN-4Pd-13Zr in Region 4. Both fuel phases (U phase and U-10Zr phase) can be observed. Some lanthanides are observed immobilized together with Pd as precipitates (e.g., Pd-Nd).

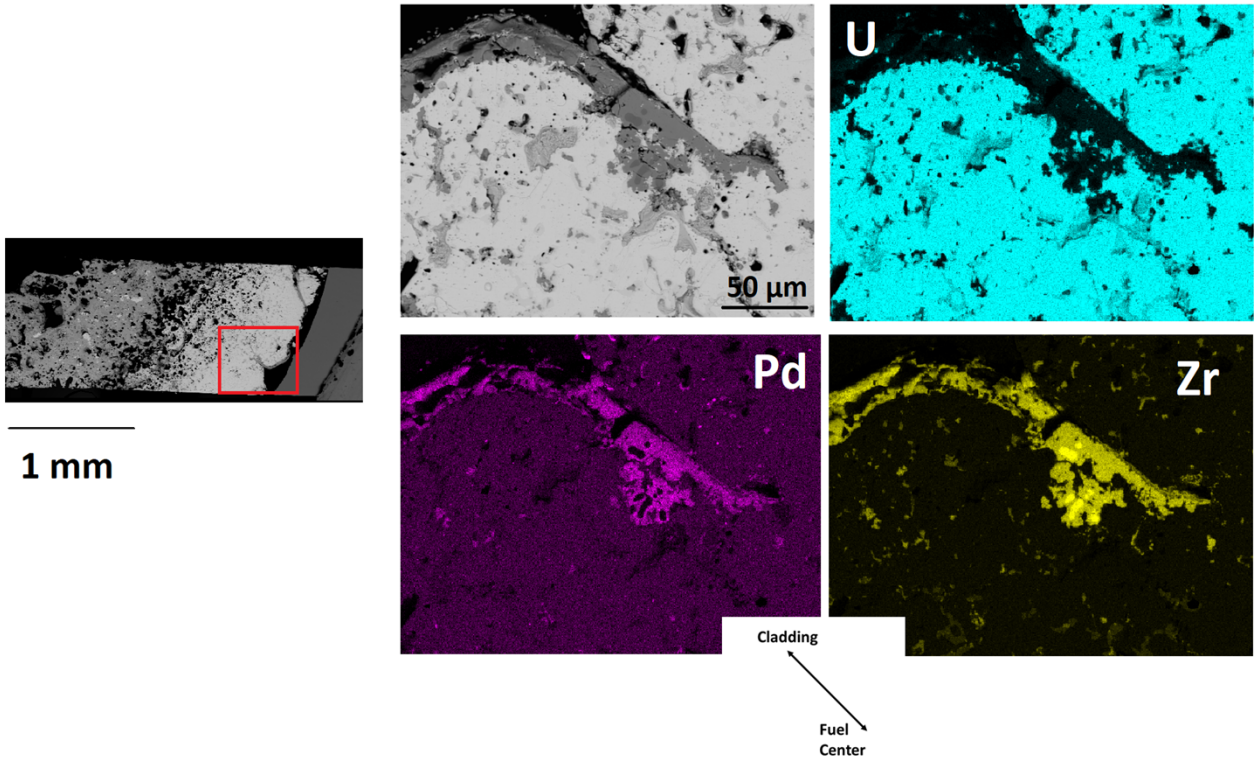

Figure 7. X-ray maps showing two phases in Region 3 of sample ANN-4Pd-10Zr, at the fuel periphery where cladding/fuel contact was expected. A U pure phase is the major component of the fuel, with a minor contribution of the U-Zr secondary phase. A Pd-Zr enriched area on the periphery of the fuel was also observed.

3.1.2 Solid fuel

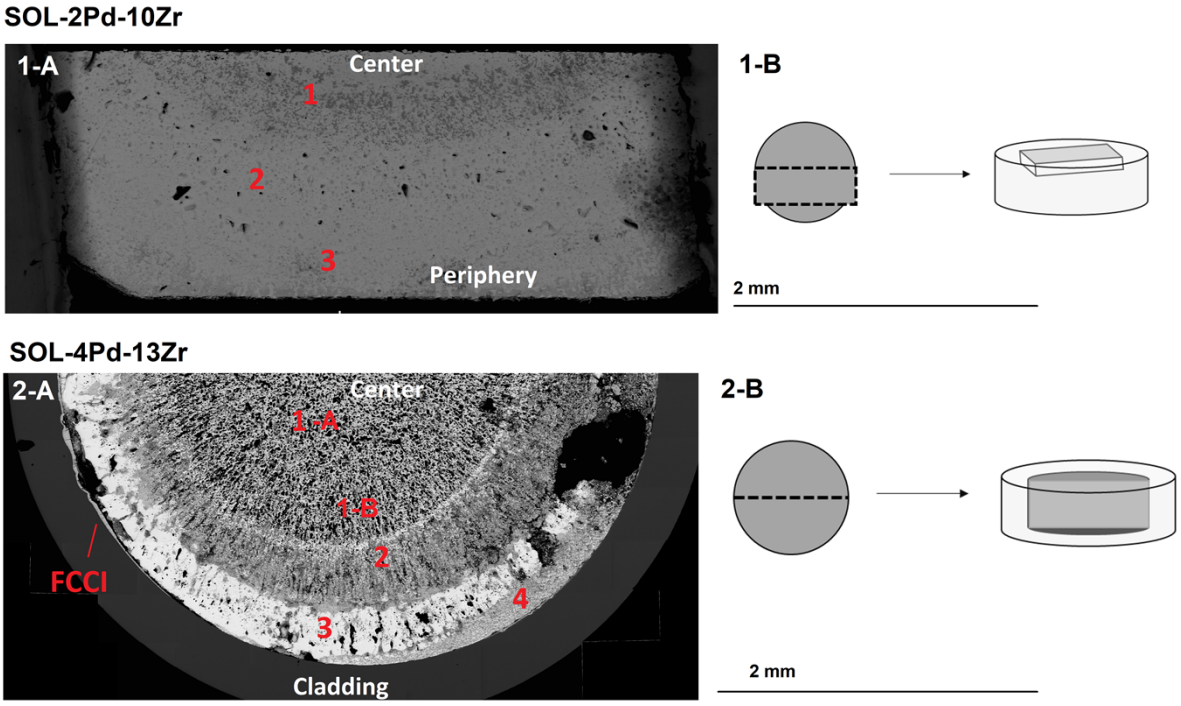

Figure 8. Overview of the microstructure in the solid samples obtained by the BSE detector for the two solid samples: 1) SOL-2Pd-10Zr and 2) SOL-4Pd-13Zr. Together with the position of their cut (1-B, 2-B). The numbers in red in the BSE images (1-A, 2-A) indicate the regions of different elemental redistribution.

The two solid-fuel samples analyzed present very different microstructures when compared to each other (Figure 8). SOL-2Pd-10Zr shows a more homogeneous contrast in the BSE image, while SOL-4Pd-13Zr presents very clearly different elemental-redistribution regions. Three regions can be observed for sample SOL-2Pd-10Zr, based on the BSE image, while for the second specimen (SOL-4Pd-13Zr), four regions redistribution can be distinguished. SOL-4Pd-13Zr presents two internal regions with dark contrast (probably related to low mass elements, Regions 1–2) and two peripherial regions with light contrast (containing high-mass elements, Regions 3–4).

Zr was observed to be enriched in the central region (see Figure 9) for both solid-fuel samples, in line with the elemental distribution of prototypical metallic fuel with a similar temperature regime, as previously described [1]. For both SOL-2Pd-10Zr and SOL-4Pd-13Zr, it was noticed that the in the central region fuel is composed of only a U-Zr phase. These samples did not show the presence of the second phase containing only U in this region. Indeed, a unique homogenous phase with U-Zr (with Zr concentration over 20 wt.%) was observed in Region 1. The solid-fuel samples differ in the following regions with SOL-4Pd-13Zr, showing also in Region 2 the presence of only the U-Zr phase (see Figure 10). In region 2, the contribution of U to the binary alloy was higher than in Region 1, as expected by the U/Zr redistribution behavior. In the peripheral region (Regions 3), SOL-4Pd-13Zr behaves very similar to ANN-4Pd-13Zr where the U phase was found to be the main phase with the presence of a minor U-Zr secondary phase. Region 4 consist finally of nearly pure U, with Zr being unalloyed to U (see Figure 11). Sample SOL-2Pd-10Zr, on the other hand, shows the Zr to be nearly all retained in the central region (Figure 9); thus, Region 2 and 3 were composed essentially of the U nearly

pure phase, with some sparse Zr precipitates. A Zr rind was observed in this sample at the edge of the fuel cross-section (Figure 9). Rinds consisting of a layer of enriched in Zr (Zr-C/Zr-Si) on the periphery of the fuel rod, have been observed to be formed during fabrication when using the injection casting method [6,31-32].

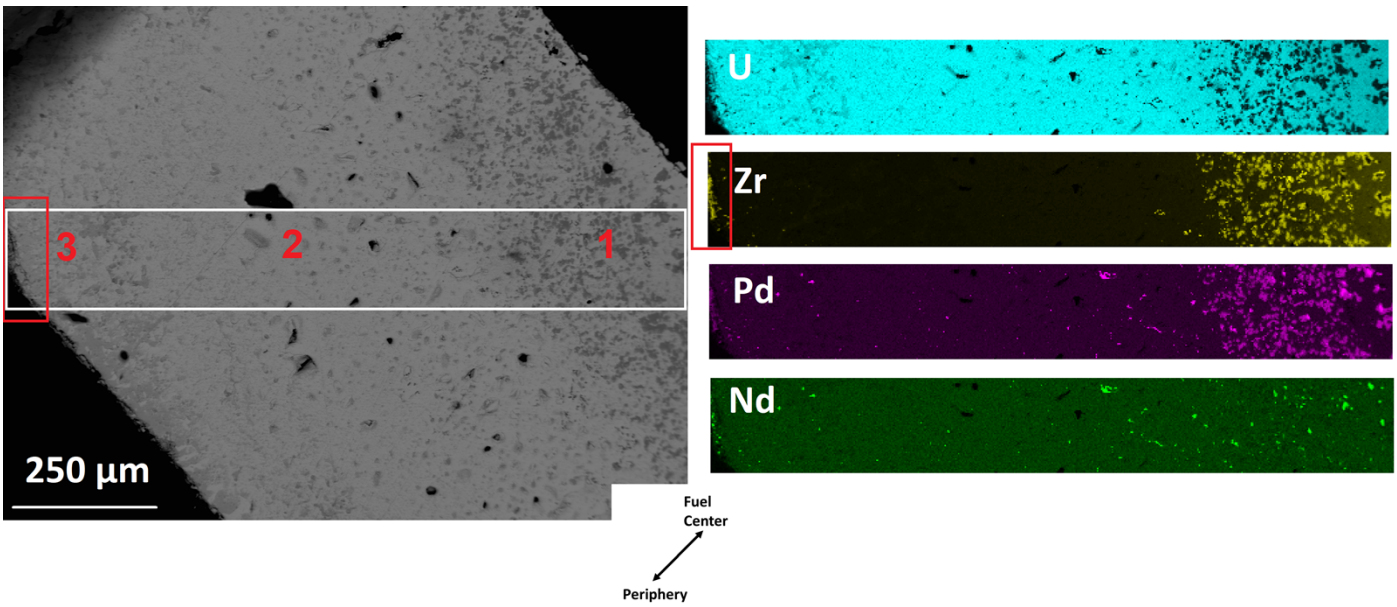

Figure 9. An example of main elements redistribution (sample SOL-2Pd-10Zr). On the left is the BSE image, with X-ray maps shown on the right. The number in red indicates the regions of different elemental redistribution shown in Figure 8. The Zr rind has been highlighted with a red rectangle.

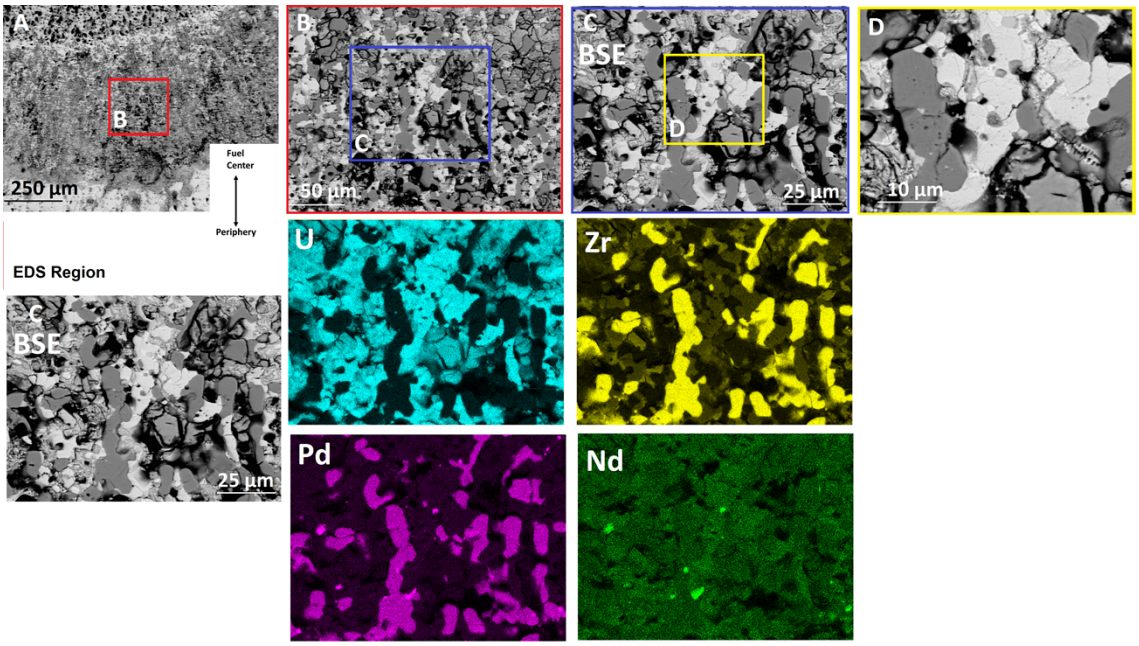

Figure 10. BSE images at different magnification for SOL-4Pd-13Zr in Region 2 (top). The colored rectangles indicate the progressive region of interest in the magnified images (from A to D). X-ray maps obtained from magnification C show the presence of only one U-Zr matrix phase by X-ray and the Pd-Zr phase.

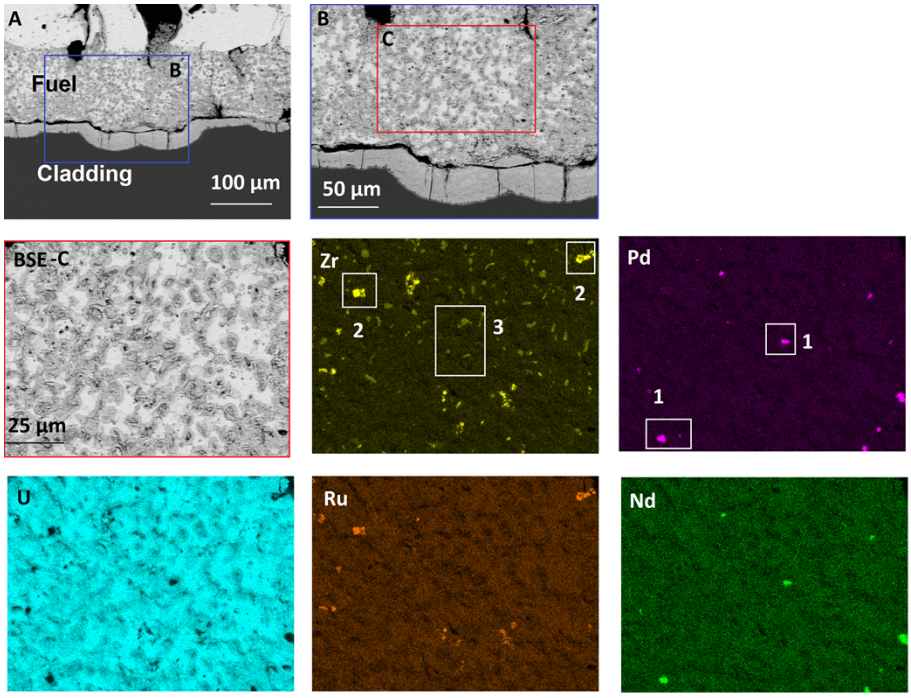

Figure 11. BSE images at different magnifications (A, B, C) for Region 4 of SOL-4Pd-13Zr and X-ray maps at the highest magnification (C). One main phase (unalloyed U) was detected. The small amount of Zr present was indeed neither associated with U or Pd Zr was found in precipitates together with Ru (2) or alone (3). Pd-Nd precipitates are observed in this region (1).

3.2 Pd behavior

The Pd added to bind lanthanides and avoid their migration to the cladding showed to combine with the lanthanides produced during reactor irradiation. However, Pd was also observed to bond strongly with the main fuel-alloying element, namely Zr (see Figure 3, Figure 4, Figure 5, Figure 7, Figure 9, Figure 10). When combined with Zr, Pd tends to form different phases [33]. In most of the samples analyzed in this work, these have been composed of 60/65 wt% Zr and 40/35 wt% Pd. This is similar to the composition of $PdZr_2$ observed in previous works [11,13]. It has been observed that this Pd-Zr phase seems to be formed the most in the central region of the fuel (Figure 9). This indicates strong redistribution during irradiation because in fabrication Pd-Zr phase were observed homogenously distributed across the full sample. This phase is not present in the peripheral region, where Pd seems to be combined mainly with lanthanides (Figure 6 and Figure 11); although, in sample ANN-4Pd-10Zr, Pd was observed to react with the Zr rind (Figure 7). As mentioned, the Zr rind is usually formed during sample fabrication [6,31-32] and it is believed to have reacted with Pd during irradiation. This rind showed a positive effect on mitigating FCCI. This effect has also been observed in previous PIE results even when Pd was not presence and the rind was composed of Zr-C/Zr-Si phases [6,31].

In sample ANN-4Pd-10Zr, a phase with higher Pd content (up to 50 wt%) was observed in the central region. In this sample, phases proved to be complex and to contain U-Zr-Pd and Fe (Figure 5) with high variation in composition. Fe indeed may have played an important role in the chemistry of this specimen (ANN-4Pd-10Zr), leading to the formation of multiple phases. As previously observed, this different chemistry may have been related to a different fabrication process, generating asymmetric behavior and leading to increased temperatures in the fuel

followed by increased Fe diffusion in the fuel. A summary of the range of compositions measured for the Pd-Zr phases in all four fuel samples is reported in Table 3.

Table 3-Example composition of the Pd-Zr phase observed in the specimen by EDS point analyses.

Samples	Composition at.%				Ratio Zr/Pd
	Pd	Zr	Fe	U	
ANN-4Pd-10Zr	19-64	35-67	0-17	0-11	0.5-3.5
ANN-4Pd-13Zr	32	67			2.09
SOL-2Pd-10Zr	37	63			1.98
SOL-4Pd-13Zr	34	66			1.94

Precipitates containing Pd, not associated with Zr, were also observed both in the center and periphery of the different fuel samples (see Figure 5, Figure 6, Figure 9, Figure 10, Figure 11). These precipitates contained lanthanides and are of great interest for fuel performance because they show that Pd has successfully reacted as intended. Data on the composition of these precipitates were difficult due to their small dimension, which leads to the influence of the surrounding matrix on the elemental analyses. These precipitates indeed showed high compositional variation by EDS point analyses. In general, it was observed that Pd composes up to 60 wt%. of the precipitates. Nd seems to be the most abundant lanthanide in these precipitates (up to 25 wt%), followed by Ce (up to 10 wt%). Pr seems to be in similar concentration in these precipitates (ca. 8 wt%), while Sm is the lowest contributor. This lanthanides composition is similar to fission products precipitates observed by Mariani et al. [9]. Although there is significant variation of composition, the EDS analyses seem to indicate the formation of 1:1 or 2:1 Pd:Ln precipitates. Phase determination of these precipitates needs further analysis with diffraction techniques, such as X-ray diffractometry or electron diffractometry in transmission electron microscopy, which could resolve their small dimension, as performed by Benson et al. [13]. Finally, sample SOL-2Pd-10Zr showed that Pd can impede the migration of lanthanides to the periphery of the fuel when lanthanides are successfully bonded to Pd (Figure 9). Indeed, most of the lanthanides were found to be concentrated in the central region together with Pd.

3.3 FCCI and cladding

FCCI was detected on the cladding side (HT-9) only on samples ANN-4Pd-13Zr and SOL-4Pd-13Zr, with interaction zones under 55 μm and under 35 μm, respectively. In sample ANN-4Pd-10Zr, FCCI was observed only on the fuel side, and limited diffusion of U in the cladding was observed. Sample ANN-4Pd-13Zr shows Fe in the central region of the fuel (Region 1), however, it is not clear the mechanism for its migration as the interaction on the fuel/cladding interface extends for only 55 μm. It must be pointed out that these analyses capture the status of fuel in a particular section, not providing in depth information on kinetics and axial behavior of components.

In the samples (ANN-4Pd-13Zr, SOL-4Pd-13Zr) where FCCI interaction was found on the cladding side, this proved to be mainly formed by U-Fe interaction, with a measured composition of UFe_2 (Figure 12). In Sample SOL-4Pd-13Zr, this FCCI layer was observed to show numerous cracks, confirming the brittle nature of the interaction layer (Figure 11). On the other hand, some limited U migration along grain boundaries in the cladding was observed in sample ANN-4Pd-10Zr but seems to be localized and did not create a uniform cladding wastage (Figure 13). For sample SOL-2Pd-10Zr, the cladding was not available for FCCI analysis.

However, no Fe was detected to have migrated into the fuel when the periphery of the fuel cross-section was analyzed. It may be inferred that the Zr rind in this sample, formed during fabrication, had a protective function. The Zr rind showed to have reacted with Pd and may have acted as a barrier for diffusion phenomena. However, in this sample (SOL-2Pd-10Zr), the lanthanides present in the external region did not seem to bond effectively with Pd, probably because most of the Pd was consumed by the interaction with the Zr rind (Figure 14). Differently to what observed in other regions and samples in which Pd was released from the Pd-Zr phase and available to react with lanthanides as expected. Indeed most of the lanthanides were observed to be effectively bonded to Pd and did not contribute to FCCI. Only in sample ANN-4Pd-13Zr was some limited localized area of the cladding found to contain Ce (Figure 15). In this area, however, the thickness of the FCCI was very small (under 5 μm). On the contrary, the solid sample SOL-4Pd-13Zr showed no Ce or other lanthanides in the cladding. In sample ANN-4Pd-10Zr (Figure 16), no RE migration was observed in the cladding. Indeed, the lanthanide precipitates were found in limited amounts in the periphery of the fuel, and were always bonded with Pd. These analyses confirmed the observation by Harp et al. [15] indicating that the lanthanide attack was lacking in the FCCI formed in these samples.

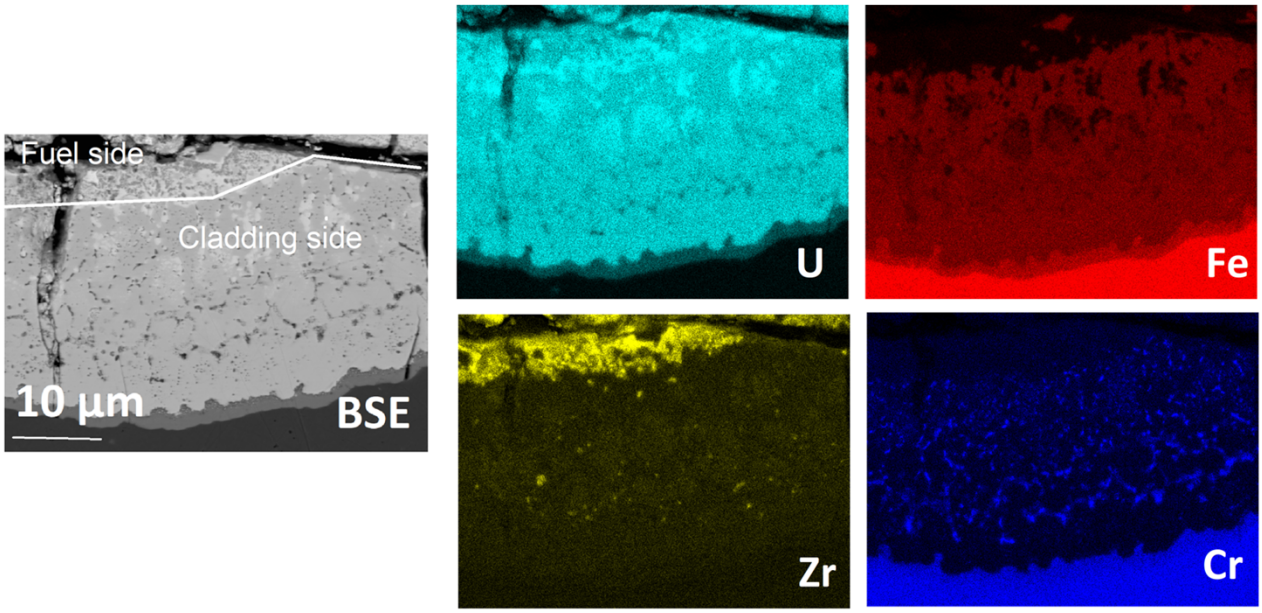

Figure 12. FCCI region of Sample SOL-4Pd-13Zr. On the cladding side, high thickness of FCCI can be observed although no lanthanide migration was observed in this area, and this reaction was created by U diffusion into the cladding and its reaction with Fe.

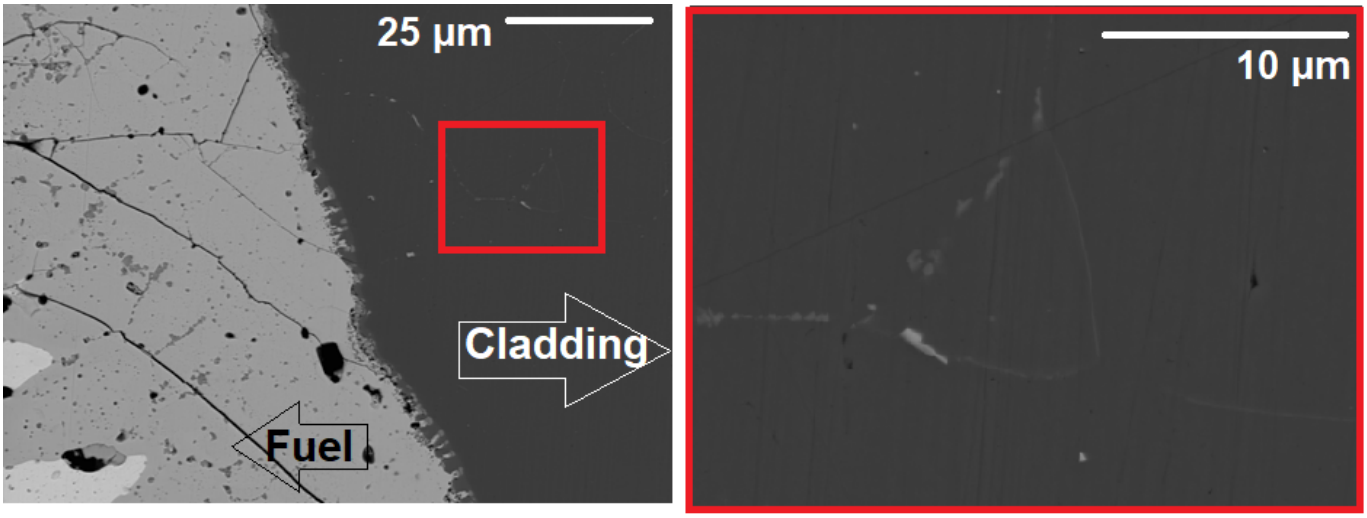

Figure 13. High-magnification BSE image of FCCI region for sample ANN-4Pd-10Zr showing limited attack of U at grain boundary, but no cladding-wastage formation. Point analyses on the grain boundary indicated U as the element present. EDS maps of a similar region is shown in Figure 16, indicating Fe is the main element responsible for the FCCI on the fuel side.

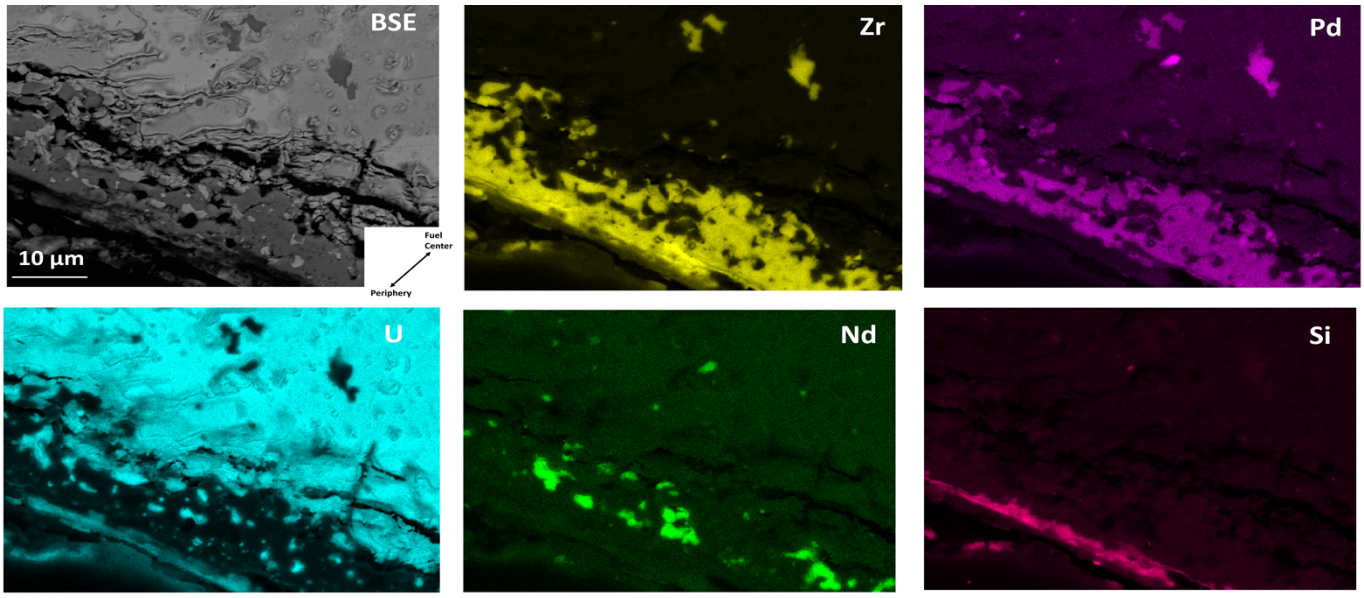

Figure 14. Fuel/cladding interaction region on fuel side showing the Pd combined with the Zr rind, which may have prevented interdiffusion (SOL-2Pd-10Zr). Nd is observed did not combine with Pd.

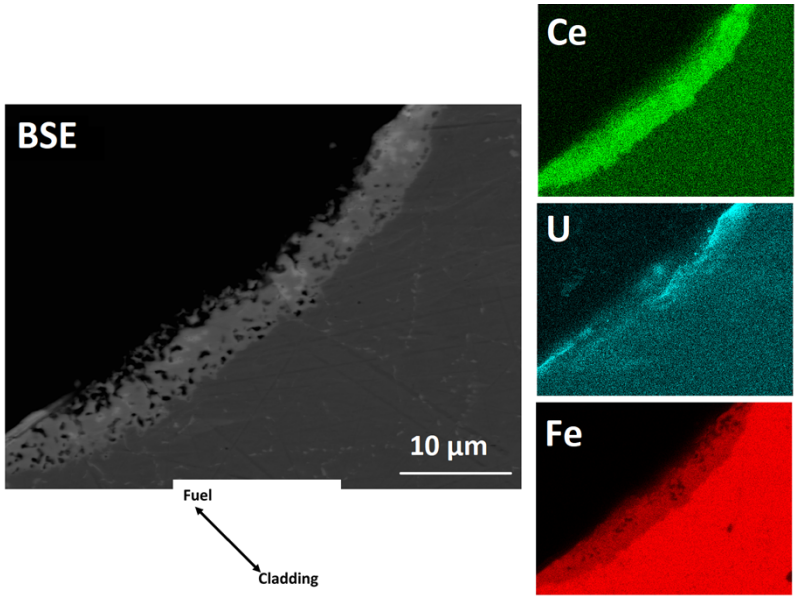

Figure 15. FCCI observed in sample ANN-4Pd-13Zr on the cladding side showing minor Ce migration in the cladding.

In samples SOL-4Pd-13Zr and ANN-4Pd-10Zr, large amounts of Fe migration into the fuel side were observed (Figure 13, Figure 16). This extended up to 50 µm in each sample. The EDS analyses indicated the compound to be formed to be possibly UFe_2 for both samples. It must be pointed out that U-Fe interaction on the fuel side for Sample SOL-4Pd-13Zr was observed only in localized areas of the fuel/cladding interface (Figure 15).

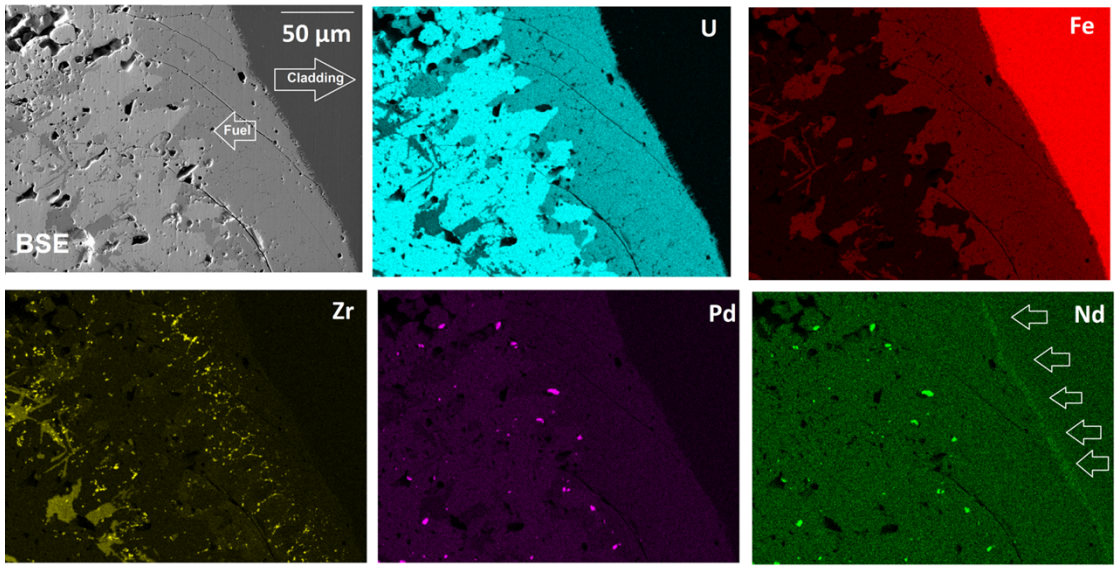

Figure 16-X-ray maps of the FCCI region for sample ANN-4Pd-10Zr. The FCCI consists of U-Fe interaction, mostly on the fuel side. Pd successfully contained the lanthanides (e.g., Nd), which do not contribute to the FCCI in this region. Note that the slight enrichment of Nd near the cladding, highlighted by the arrows, is related to Cr interference. Finally, no major Pd-Zr phase is observed in the periphery of the fuel.

4. Discussion

The behavior of Pd was investigated by SEM in different metallic fuel specimens to evaluate its effectiveness in preventing lanthanide attack on the cladding under typical reactor conditions. Although the samples had similar burn ups and calculated temperatures, different phases and microstructures were observed to form, likely owing to different sample-fabrication conditions and composition. Moreover, some limitations of this study may be related to the unforeseen behavior of sample ANN-4Pd-10Zr which may be related to the fabrication process, involving a significant gap (>50 μm) between the fuel slug and the cladding. This may have deteriorated the fuel performance introducing a data gap in these analyses and lead to Fe being a major influence on fuel chemistry.

As predicted by Mariani et al. [9] and observed in previous PIE by Harp et al. [15, 17], Pd forms high-temperature thermodynamically stable intermetallic phases with Zr alloying element of the fuel matrix. Such phases were observed and analyzed in this study. The Pd-lanthanide intermetallic phases were previously reported to be more thermodynamically favorable than Pd-Zr compounds and were expected to decompose during irradiation. In these analyses, it was observed that Pd is not completely released during reactor irradiation from the Pd-Zr phases. This may be related to the low burn up levels (under 3% FIMA) and, thus, to minor concentration of lanthanides in the fuel matrix available for reaction with Pd. Indeed, only in limited areas was it observed that Pd had left the Zr matrix to combine with lanthanide precipitates effectively. The Pd-Zr phases were mostly found in the central region, where both Pd and Zr are more abundant. This may be due to redistribution of Zr in metallic fuel and the affinity of Pd with this element. While in the outer region, limited Pd was found and mostly alloyed with lanthanides since lanthanides are reported to migrate to the periphery of the fuel during irradiation.

The formation of Pd-Zr intermetallic phases can have a detrimental effect on fuel performance. As when U is unalloyed the fuel solidus temperature is lowered and U-Fe interactions increase at temperatures over 550°C, as observed in previous studies [10,15,17,23]. Such extensive interaction of U-Fe has been detected in these samples. Indeed, studies have indicated that in normal operation FCCI in U-Zr alloy should not be dominated by U-Fe interaction, but by the lanthanide attack [34]. Moreover, FCCI is generally expected at higher burnup over 5% FIMA, while these studies show FCCI even at burnup under 3% FIMA that may be attributed to the Pd-Zr interaction and the increased unalloyed U. In the AFC-3C/D campaign, it was decided to increase the Zr content in the matrix (from 10 wt% to 13 wt%) with respect to the previous campaigns (AFC-3A/3B) in order to address these issues attributed to this Pd-Zr interaction. However, the increase of Zr to 13 wt% has been observed in this study to mitigate only partially this effect; as nearly pure U was still present, and FCCI with U-Fe interaction present, mostly on the cladding side. The Zr increase in the matrix seems, moreover, to have played an important role on phase formation. While the microstructure was different for sample SOL-4Pd-13Zr and ANN-4Pd-13Zr, similar phases were indeed observed in these samples (Pd-Zr, U-Zr, unalloyed U). These presumptive phases are consistent with the ones identified in previous fresh fuel analyses (PdZr2, δ-UZr2, α-U) [8, 9, 11]. The formation of α-U observed in widely in PIE has been demonstrated to be thermodynamic favorable recently by the CALPHAD method [35]. Ternary phases (U-Zr-Pd) were not observed in line with the work of Benson et al. [10]. Indeed, ternary phases observed by Benson et al. [10] during casting were reported to be eliminated by annealing; thus, they should not be present after reactor irradiation at over 500°C. Sample SOL-2Pd-10Zr showed an extensive area of nearly pure U. While the chemistry of sample ANN-4Pd-10Zr was complicated by the high influence of Fe and cannot be thus directly compared with the other samples.

In this study, Pd addition in metallic fuel successfully mitigated lanthanide attack to the cladding. In these analyses, many lanthanides were immobilized by Pd in precipitates. Some even mostly in the center of the fuel, as observed in SOL-2Pd-10Zr. This confirms that Pd acts by the desired mechanism of lanthanide migration control [9,13]. The Pd-Ln precipitates have been previously reported [10, 11] to range from Pd:Ln, 1:1, 2:1, 3:2, 4:3 and 3:7. In the previous analyses, it seems that 1:1 and 3:7 were the prevalent ratios and clearly visible by SEM, while the other phases were smaller and identifiable only by transmission electron microscopy analysis. In this study, however, the high variation in the data seems to indicate the formation of 1:1 or 2:1 Pd:Ln precipitates. These Pd:Ln compositions have been confirmed by recent thermo-equilibrium calculations to be stable in the U-10Zr fuel matrix [35]. SOL-2Pd-10Zr, which had 2 wt% Pd showed some lanthanides to have reached the periphery of the fuel without binding to Pd. This may be detrimental for mitigating FCCI and may call for higher Pd content, control of the Pd-Zr reaction, or different Pd distribution (as Pd reacted in the external region with the Zr rind in this sample).

In these samples, lanthanide attack on the cladding was indeed limited. Lanthanide diffusion into the cladding was observed only for one sample (ANN-4Pd-13Zr), in a limited region, and at a minimal depth (<5 μm). This sample showed Ce alone to be present in the cladding. This may be caused by the fact that Ce is observed to be among the lanthanides that show a higher diffusion into Fe [13], due to its fission yield and diffusion kinetics [7]. A particular effect observed on sample SOL-2Pd-10Zr was the formation of a Pd-Zr barrier on the outer diameter of the fuel, which seem to have acted as barrier to lanthanide attack. A similar phenomenon was observed in Ref. [14], in which the $PdZr_2$ precipitates have been observed to act as a barrier towards Fe diffusion in the fuel.

In the sample (ANN-4Pd-10Zr) where FCCI on the fuel side was extensive. This was caused by high Fe diffusion. The FCCI was detected to be mostly composed of UFe_2, in line with previous observation by Xie et al. [14]. Recent calculations by Geiger et al. [35] also predict the formation of ternary phases U-Fe-Zr, together with UFe_6 and $FeZr_2$ which were not observed in this work. A summary of the main observation for each sample is presented in Table 4.

Table 4- Summary of main observations from the performance of the analyzed fuels with Pd.

Sample	Pd/Ln behavior	Pd/Zr behavior	FCCI	Other
ANN-4Pd-10Zr	Reacted	Yes, influenced by Fe	Extensive fuel side	Fe influence, Zr-Pd Rind
ANN-4Pd-13Zr	Reacted	Yes 1:2	Cladding Side	
SOL-2Pd-10Zr	Reacted	Yes 1:2	Fuel Side	Some unreacted Ln reach periphery, Zr-Pd rind
SOL-4Pd-13Zr	Reacted	Yes 1:2	Cladding Side	

Following these observations of some detrimental effect of Pd on fuel performance, other candidates, Sb and Sn, have been proposed as an additive aimed at mitigating Ln attack on cladding. Sb and Sn have shown promising results in modelling and simulation, in out-of-pile tests, showing a preferential binding for lanthanides over Zr [36-37].

5. Conclusions and future work

In this work, irradiated metallic fuel containing Pd as an additive for FCCI mitigation was, for the first time, investigated via SEM. Two different fuel designs and different Pd compositions were analyzed. The efficacy of Pd additive is still not fully understood. While the desired mitigation of the migration of lanthanides to the cladding was observed, an extensive formation of Pd-Zr phases was detected. The Pd-Zr reaction can leave high fractions of U unalloyed (as observed by the high amount of nearly pure U in the fuel matrix), which can be detrimental to fuel performance, both increasing U-Fe interaction at the cladding interface and lowering the fuel's melting point. Even the increase of Zr from 10 wt% to 13 wt% was not successful in fully mitigating this effect. Although these phases were already observed in the fabrication of this fuel form, it was expected that, during irradiation, the Pd will be released from Pd-Zr intermetallics to interact with lanthanides. This phenomenon may be mitigated at higher burn-up where more Ln are present, which may lead to Zr to react with Ln rather than Pd. Thus, the use of Pd as an additive requires further studies. Other candidates have also been proposed as additive for FCCI mitigation and Ln binding, such as Sb and Sn which should present less reactivity towards Pd.

Most of the lanthanides, however, did bind effectively to Pd, and the Pd-lanthanide observed phases during irradiation match the one observed in fresh fuel (1:1) by SEM characterization in previous studies. Pd concentration of 4 wt%. showed a slightly better performance in binding lanthanides, as some lanthanide precipitates in the 2 wt% sample were observed to reach the cladding without binding with Pd.

In future studies, ternary fuel alloys should also be tested to understand the influence of Pu on phases formed and FCCI. The irradiation of different additives in metallic fuel and use of liners should be also further investigated as means of providing FCCI mitigation for increasing burnup of metallic fuels. Moreover, additives should also be investigated for other considerations, such as their neutronic performance and their influence on fuel-fabrication and fuel-cycle costs.

Acknowledgments

Much of this work was supported through the Department of Energy, Advanced Fuels Campaign, under DOE Idaho Operations Office Contract DE-AC07-05ID14517. Accordingly, the U.S. Government retains and the publisher, by accepting the article for publication, acknowledges that the U.S. Government retains a nonexclusive, paid-up, irrevocable, world-wide license to publish or reproduce the published form of this manuscript, or allow others to do so, for U.S. Government purposes. Mr. A. Winston and Mr. A. Pomo are thanked for extensive sample preparation. Dr. D. Porter is thanked for the fruitful discussion. The Electron Microscopy Laboratory (EML) and Dr. J.-F. Jue are especially acknowledged for experiment coordination and for the scientific and technical support.

U. S. Department of Energy Disclaimer

Government or any agency thereof.

Data availability statement

The raw/processed data required to reproduce these findings cannot be shared at this time due to legal or ethical reasons.

References

[1] T. Ogata, Metal Fuel, Compr. Nucl. Mater., Elsevier, 2012: 1–40, Ed. R. Konings, 10.1016/B978-0-08-056033-5.00049-5.

[2] T. Sofu, A review of inherent safety characteristics of metal alloy sodium-cooled fast reactor fuel against postulated accidents, Nucl. Eng. Technol. 47, no. 3, 2015: 227–239, 10.1016/j.net.2015.03.004.

[3] W.J. Carmack, D.L. Porter, Y.I. Chang, S.L. Hayes, M.K. Meyer, D.E. Burkes, C.B. Lee, T. Mizuno, F. Delage, and J. Somers, Metallic fuels for advanced reactors, J. Nucl. Mater. 392, no. 2, 2009: 139–150, 10.1016/j.jnucmat.2009.03.007.

[4] B. D. Middleton, E. J. Parma, T. J. Olivier, J. Phillips, and J. L. Lachance, The Development of a Realistic Source Term for Sodium-Cooled Fast Reactors: Assessment of Current Status and Future Needs, Sandia National Laboratory technical report, Sandia, USA., vol. SAND2011-3, (2011). Available on https://prod-ng.sandia.gov/techlib-noauth/access-control.cgi/2011/113404.pdf

[5] D.C. Crawford, D.L. Porter, and S.L. Hayes, Fuels for sodium-cooled fast reactors: US perspective, J. Nucl. Mater. 371, nos. 1–3, 2007: 202–231, 10.1016/j.jnucmat.2007.05.010.

[6] D.D. Keiser, 3.15—Metal Fuel-Cladding Interaction, in Rudy J.M. Konings (ed.), Comprehensive Nuclear Materials, Elsevier, 2012, Pages 423–441, 10.1016/B978-0-08-056033-5.00067-7.

[7] E.B. Lee, B.O. Lee, W.Y. Shim, and J.H. Kim, Correlation between rare earth elements in the chemical interactions of HT9 cladding, Nucl. Eng.Tech. 50, no. 6, 2018: 915–922, 10.1016/j.net.2018.04.015.

[8] Y. Xie, J. Zhang, X. Li, J.P. Isler, M. T. Benson, R.D. Mariani, and C. Unal, Lanthanide migration and immobilization in metallic fuels, Progr. Nucl. Energy 109, 2018: 233–238, 10.1016/j.pnucene.2018.08.019.

[9] R.D. Mariani, D.L. Porter, T.P. O'Holleran, S.L. Hayes, and J.R. Kennedy, Lanthanides in metallic nuclear fuels: Their behavior and methods for their control, J. Nucl. Mater. 419, nos. 1–3, 2011: 263–271, 10.1016/j.jnucmat.2011.08.036.

[10] M.T. Benson, L. He, J. A. King, and R.D. Mariani, Microstructural characterization of annealed U-12Zr-4Pd and U-12Zr-4Pd-5Ln: Investigating Pd as a metallic fuel additive, J. Nucl. Mater. 502, 2018: 106-112, 10.1016/j.jnucmat.2018.02.012.

[11] Y. Xie, and M. T. Benson, Microstructure and diffusion behavior of uranium fuel with minor additives, J. Nucl. Mater. 535, 2020: 152200, 10.1016/j.jnucmat.2020.152200.

[12] M.T. Benson, L. He, J.A. King, R.D. Mariani, A.J. Winston, and J.W. Madden, Microstructural characterization of as-cast U-20Pu-10Zr-3.86Pd and U-20Pu-10Zr-3.86Pd-4.3Ln, J. Nucl. Mater., 508, 2018: 310–318, 10.1016/j.jnucmat.2018.05.062.

[13] M T. Benson, J. M. Harp, Y. Xie, T. Yao, K. R. Tolman, K.E. Wright, J.A. King, A.I. Hawari, and Q. Cai, Out-of-pile and postirradiated examination of lanthanide and lanthanide-palladium interactions for metallic fuel, J. Nucl. Mater. 544, 2021:152727, 10.1016/j.jnucmat.2020.152727

[14] Y. Xie, M.T. Benson, L. He, J.A. King, R.D. Mariani, and D.J. Murray, Diffusion behaviors between metallic fuel alloys with Pd addition and Fe, J. Nucl. Mater. 525, 2019: 111-124, 10.1016/j.jnucmat.2019.07.028.

[15] J. M. Harp, H. J. M. Chichester, and L. Capriotti, Postirradiation examination results of several metallic fuel alloys and forms from low burnup AFC irradiations, J. Nucl. Mater. 509, 2018: 377–391, 10.1016/j.jnucmat.2018.07.003.

[16] S. L. Hayes, J. M. Harp, H. J. M. Chichester, R. S. Fielding, R. D. Mariani, and W. J. Carmack, Advances in Metallic Fuels for High Burnup and Actinide Transmutation, 2016, INL/CON-16-38752, Conference: 14th Information Exchange Meeting on Actinide and Fission Product Partitioning and Transmutation, San Diego, USA, October 17–20, 2016 https://www.osti.gov/biblio/1358285.

[17] J. M. Harp, L. Capriotti, and F. Cappia, Baseline Postirradiation Examination of the AFC-3C, AFC 3D, and AFC-4A Experiments, INL/EXT-18-51447, Idaho National Laboratory technical report, Idaho Falls, USA, Revision 0, 2018. https://doi.org/10.2172/1498255

[18] R. S. Fielding, P. A. Hansen, T. A. Hyde, and J. Maupin, Fabrication Report for the FY11 Phases of the AFC-3A and 3B Irradiation Experiments, Idaho National Laboratory technical report, Idaho Falls, USA,., INL/LTD-11e23158, 2011.

[19] T. P. O'Holleran, C. A. Papesch, L. N. Squires, T. A. Hyde, J. R. Kennedy, and T. Hartmann, AFC-3 Fuel Characterization, Idaho National Laboratory technical report, Idaho Falls, USA, INL/LTD-12-24346, 2012.

[20] J. M. Harp, S. L. Hayes, P. G. Medvedev, D. L. Porter, and L. Capriotti, Testing Fast Reactor Fuels in a Thermal Reactor: A Comparison Report, Idaho National Laboratory technical report, Idaho Falls, USA, INL/EXT-17-41677 Revision 0, 2017.

[21] M. Smith, ABAQUS/Standard User's Manual, Version 6.14, Dassault Systèmes Simulia Corp, (2014). Available at http://130.149.89.49:2080/v6.14/pdf_books/ANALYSIS_4.pdf

[22] G. L. Hofman, S. L. Hayes, and M. C. Petri, Temperature gradient driven constituent redistribution in U-Zr alloys, J. Nucl. Mater. 227, no. 3, 1996: 277–286, 10.1016/0022-3115(95)00129-8.

[23] J. M. Harp, D. L. Porter, B. D. Miller, T. L. Trowbridge, and W. J. Carmack, Scanning electron microscopy examination of a Fast Flux Test Facility irradiated U-10Zr fuel cross section clad with HT-9, J. Nucl. Mater. 494, 2017, 227–239, 10.1016/j.jnucmat.2017.07.040.

[24] L. Capriotti, and J. M. Harp, Characterization of a minor actinides bearing metallic fuel pin irradiated in EBR-II, J. Nucl. Mater. 539, 2020: 152279, 10.1016/j.jnucmat.2020.152279.

[25] F. G. Di Lemma, K. E. Wright, L. Capriotti, A. X. Zabriskie, A. J. Winston, C. B. Jensen, and D. M. Wachs, Investigation of fuel microstructure at the top of a metallic fuel pin after a reactor overpower transient, J. Nucl. Mater. 544, 2021: 152711, 10.1016/j.jnucmat.2020.152711

[26] S. Brémier, K. Inagaki, L. Capriotti, P. Poeml, T. Ogata, H. Ohta, and V. V. Rondinella, Electron probe microanalysis of a METAPHIX UPuZr metallic alloy fuel irradiated to 7.0 at.% burn-up, J. Nucl. Mater. 480, 2016: 109–119, 10.1016/j.jnucmat.2016.07.060

[27] Fast Reactor Working Group, Nuclear Metal Fuel: Characteristics, Design, Manufacturing, Testing, and Operating History, Technical Report, White Paper 18-01, June 2018, Available at

https://www.nrc.gov/docs/ML1816/ML18165A249.pdf

[28] J. Galloway, C. Unal, N. Carlson, D. Porter, and S. Hayes, Modeling constituent redistribution in U–Pu–Zr metallic fuel using the advanced fuel performance code BISON, Nucl. Eng. Des., 286, 2015, 1-17, https://doi.org/10.1016/j.nucengdes.2015.01.014.

[29] J. M. Harp, D. L. Porter, B. D. Miller, T. L. Trowbridge, and W. J. Carmack, Scanning electron microscopy examination of a Fast Flux Test Facility irradiated U-10Zr fuel cross section clad with HT-9, J. Nucl. Mater. 494, 2017: 227–239, 10.1016/j.jnucmat.2017.07.040.

[30] G. L. Beausoleil II and G. L. Povirk and B. J. Curnutt, A Revised Capsule Design for the Accelerated Testing of Advanced Reactor Fuels, Nucl. Tech., 206, 3, 444-457, 2020 10.1080/00295450.2019.1631052.

[31] F. Di Lemma, and D. L. Porter, Secondary Phase Objects in As-cast U-10 wt% Zr, Idaho National Laboratory technical report, Idaho Falls, USA, INL/EXT-17-41918-Rev002, (2017). doi:10.2172/1482120

[32] S. Kaity, J. Banerjee, S.C. Parida, A. Laik, C.B. Basak, and V. Bhasin, Studies on fuel-cladding chemical interaction between U−10 wt%Zr alloy and T91 steel, J. Nucl. Mater. 513, 2019,16-32, 10.1016/j.jnucmat.2018.10.041.

[33] H. Okamoto, Pd-Zr (Palladium-Zirconium), J. Phase Equilib. Diffus. 30, 2009: 413–414, 10.1007/s11669-009-9542-x

[34] J. M. Harp, L. Capriotti, D. L. Porter, and J. I. Cole, U-10Zr and U-5Fs: Fuel/cladding chemical interaction behavior differences, J. Nucl. Mater. 528, 2020: 151840, 10.1016/j.jnucmat.2019.151840.

[35] E. Geiger, C. Guéneau, E.C. Corcoran, and M.H.A. Piro, Thermodynamic investigations of fuel-cladding chemical interaction in U-5Fs and U-10Zr metallic fuels with the TAF-ID, Nucl. Mater. 551, 2021, 152981, https://doi.org/10.1016/j.jnucmat.2021.152981.

[36] Y. Xie, M. T. Benson, J. A. King, R. D. Mariani, and J. Zhang, Characterization of U-Zr fuel with alloying additive Sb for immobilizing fission product lanthanides, J. Nucl. Mater. 498, 2018: 332–340, 10.1016/j.jnucmat.2017.10.039.

[37] M. T. Benson, J. A. King, and R. D. Mariani, Investigation of Tin as a Fuel Additive to Control FCCI, Materials Society T. (eds) TMS 2018 147th Annual Meeting & Exhibition Supplemental Proceedings. TMS 2018. 695-702. The Minerals, Metals & Materials Series. Springer, Cham. 10.1007/978-3-319-72526-0_65